Numerical Study of the Turbulent Flow Past an Airfoil with Trailing Edge Separation

C. M. Rhie*
Detroit Diesel Allison, Indianapolis, Indiana
and
W. L. Chow†
University of Illinois at Urbana-Champaign, Urbana, Illinois

A finite volume numerical method is presented for the solution of the two-dimensional incompressible, steady Navier-Stokes equations in general curvilinear coordinates. This method is applied to the turbulent flows over airfoils with and without trailing edge separation. The k-ϵ model is utilized to describe the turbulent flow process. Body-fitted coordinates are generated for the computation. Instead of the staggered grid, an ordinary grid system is employed for the computation and a specific scheme is developed to suppress the pressure oscillations. The results of calculations are compared with the available experimental data.

Nomenclature

A_E, A_W, A_N, A_S, A_P = coefficients in the general finite difference equations
E = constant in the law of the wall
G_1, G_2 = convective terms normal to grid cell boundaries
k = turbulence kinetic energy
p = nondimensionalized pressure
P = rate of production of the turbulence kinetic energy
Re_C, Re_D = Reynolds numbers based on characteristic lengths
S^ϕ = source term in the finite difference equation for the general scalar ϕ
u, v = x and y components of the nondimensional velocities
x, y = nondimensional Cartesian coordinates
y^+ = nondimensionalized boundary-layer coordinate
α, β, γ = coordinate transformation parameters
Γ^ϕ = effective diffusity for the general scalar ϕ
$\delta\xi, \delta\eta$ = finite difference mesh spacings in ξ and η directions in the transformed plane
$\Delta\xi, \Delta\eta$ = cell boundary sizes in ξ and η directions in the transformed plane
ϵ = turbulence energy dissipation
κ = constant in the law of the wall
μ, μ_t = laminar and turbulent viscosities
ξ, η = nondimensional natural coordinates
ρ = nondimensional density
$\sigma_k, \sigma_\epsilon$ = effective Prandtl numbers for the turbulence kinetic energy and the turbulence energy dissipation
τ_{ij} = tensor notation of the nondimensional shear stress
ϕ = general scalar quantity

Presented as Paper 82-0998 at the AIAA/ASME Third Joint Thermophysics, Fluids, Plasma and Heat Transfer Conference, St. Louis, Mo., June 7-11, 1982; submitted June 17, 1982; revision received Nov. 22, 1982.

*Senior Project Engineer, Analytical Mechanics Department. Member AIAA.
†Professor of Mechanical Engineering. Associate Fellow AIAA.

Introduction

NUMERICAL simulation of flow past airfoils is important in the aerodynamic design of aircraft wings and turbomachinery components. These lifting devices often attain optimum performance at the condition of "onset of separation." Thus, separation phenomena must be dealt with if the analysis is aimed at practical applications.

When airfoils operate at small angles of attack, the viscous effects introduce only minor modifications to the inviscid flow. In this case, an ordinary boundary-layer analysis is adequate to describe the viscous flow behavior within the framework of "weak" viscid-inviscid interaction. However, when the angle of attack is increased, separation usually occurs which significantly alters the inviscid flowfield and the flow exhibits a "strong" viscid-inviscid interaction. One effective way to deal with this latter situation is to carry out a large-scale numerical calculation on the basis of the turbulent Navier-Stokes equations. Although many attempts have been made to solve attached flows over airfoils using the Navier-Stokes equations (see, for example, Wu et al.,[1] Steger,[2] and Gibeling et al.[3]), no significant progress has been made in the solution of flows with separation. Most of the existing methods incorporating simple turbulence models are not applicable to turbulent separating flows. In an effort to overcome this limitation, a two-equation model (k-ϵ model) was pursued recently by Shamroth and Gibeling,[4] and numerical difficulties were reported. The present study is a preliminary investigation into the problem of calculating separating turbulent flows over an airfoil using a two-equation turbulence model (k-ϵ).

The k-ϵ turbulence model has been used with elliptic solution techniques to predict near-wake flows. However, these schemes are applied only to the near-wake region where inlet boundary conditions are provided experimentally. For example, Pope and Whitelaw[5] started the calculation behind the trailing edge of a body in their study of near-wake flows. The inlet boundary conditions at the trailing edge had to be supplied from experimental data when available, or by intuition. In their work, they showed the extreme sensitivity of the downstream flowfield especially to the transverse velocity profile adopted at the trailing edge. Consequently, they could not really assess the performance of the k-ϵ model. Hah and Lakshminarayana[6] tried to predict the near wake of a single airfoil. Sufficient experimental information was provided at the inlet boundary located immediately behind the trailing edge. Although this technique was useful, the fact remains that a single method should be used for the whole flow region

without relying on any experimental information. The present study is aimed at examining the adequacy of the numerical calculation with the k-ϵ model to fulfill this need.

Computational Methods

Although the general scheme of the present method follows essentially the original Navier-Stokes solution procedure by Caretto et al.[7] (SIMPLE method), this procedure, together with its later development (TEACH code), suffers severely from geometric limitations since the equations were written in Cartesian or cylindrical polar coordinates. Application of this method to curved surfaces such as airfoils must involve interpolation between grid points not coincident with the boundaries. This may adversely affect the accuracy of the solution. In the present study, this geometric limitation is removed by adopting a general curvilinear coordinate system.

There were other attempts to develop solution techniques using the curvilinear system of coordinates. Pope[8] used a procedure for flows with recirculation by presenting the conservation equations in an orthogonal coordinate system, and an orthogonal grid system is therefore required. Demirdzic et al.[9] developed an arbitrary mesh finite volume method. They presented the equations in terms of arbitrary contravariant curvilinear velocity components. This method has the flexibility in application to general geometries. However, the semistrong conservation form of the governing equation was used. The alternative of using the Cartesian velocity components would present itself in the strong conservation form. Hirt et al.[10] developed the arbitrary Lagrangian-Eulerian (ALE) finite volume procedure in this category. In this scheme, velocity-pressure decoupling effects are observed as a result of the grid arrangement where the pressure is defined in the center of the cell while u and v velocity components are defined at the corners. This approach also involves a very complicated solution procedure.

The present method deals with the Cartesian velocity components and all the variables are located at the common grid positions as opposed to staggered grid arrangements employed by other users of this approach.[7-10] The velocity and pressure are coupled by a simple but effective scheme. The method is aimed at the future application to complex three-dimensional turbulent flow computations.

Theoretical Formulation

Governing Equations

For steady-mean flow, the time-averaged continuity equation and the Navier-Stokes equation, in conjunction with the isotropic turbulent viscosity hypothesis, are written in a Cartesian tensor form

$$\partial/\partial x_i \rho u_i = 0 \tag{1}$$

$$(\partial/\partial x_i)\rho u_i u_j = -\partial p/\partial x_j + (\partial/\partial x_i)\left[(\mu+\mu_t)\times(\partial u_i/\partial x_j + \partial u_j/\partial x_i)\right] - 2/3\rho k\delta_{ij} \tag{2}$$

where ρ is the mean density, u_j the mean velocity, and p the mean pressure. From the k-ϵ turbulence model,[11] the turbulent viscosity μ_t is given by

$$\mu_t = C_\mu \rho k^2/\epsilon \tag{3}$$

where k is the turbulence kinetic energy and ϵ is the turbulence energy dissipation.

The model is then composed of two equations; one for k and another for ϵ presented as follows:

$$\frac{\partial}{\partial x_i}\rho u_i k = \frac{\partial}{\partial x_i}\left(\frac{\mu_t}{\sigma_k}\frac{\partial k}{\partial x_i}\right) + P - \rho\epsilon \tag{4}$$

$$\frac{\partial}{\partial x_i}\rho u_i \epsilon = \frac{\partial}{\partial x_i}\left(\frac{\mu_t}{\sigma_\epsilon}\frac{\partial \epsilon}{\partial x_i}\right) + \frac{\epsilon}{k}(C_1 P - C_2\rho\epsilon) \tag{5}$$

where $P\ (=\overline{-\rho u_i' u_j'}\partial u_j/\partial x_i)$ is the rate of production of turbulence kinetic energy. This model contains five empirical constants which assume the following values:

$$C_\mu = 0.09, \quad C_1 = 1.45, \quad C_2 = 1.90, \quad \sigma_k = 1.0, \quad \sigma_\epsilon = 1.3 \tag{6}$$

The turbulence scalar transport equations [Eqs. (4) and (5)], are only valid for fully turbulent regions. An additional model must be introduced to treat the laminar sublayer region. The wall function method[12] is used in the present study to eliminate the large number of grid points needed to resolve the laminar sublayer. The following functions are used to bridge the near-wall region:

$$\tau_w = \frac{u_p}{y_p}\frac{\mu y_p^+}{\kappa^{-1}\ell n(E y_p^+)} \tag{7}$$

where $y_p^+ = \rho(k_p C_\mu^{1/2})^{1/2} y_p/\mu$

$$\epsilon_p = (C_\mu^{1/2} k_p)^{3/2}/\kappa y_p \tag{8}$$

$$\int_0^{y_p} \epsilon dy = (C_\mu^{1/2} k_p)^{3/2}\frac{1}{\kappa}\ell n(E y_p^+) \tag{9}$$

$$\left.\frac{dk}{dy}\right|_w = 0 \tag{10}$$

Here, y is the conventional coordinate normal to the wall and τ_w is the wall shear stress. The subscript p refers to the grid node next to the wall; κ and E are the constants from the law of the wall, with values of 0.4 and 8.8, respectively. It should be mentioned that this model is not capable of dealing with laminar and transition regions. The present study pays specific attention to the shear layer interaction and its subsequent relaxation in the near wake. It is expected that the leading edge transition process will not significantly affect the downstream flow condition of the present problem.

Transformation of the Basic Equations

The set of conservation equations typically can be written in the Cartesian system of coordinates for a scalar variable as

$$\frac{\partial}{\partial x}(\rho u\phi) + \frac{\partial}{\partial y}(\rho v\phi) = \frac{\partial}{\partial y}\left(\Gamma^\phi\frac{\partial\phi}{\partial x}\right) + \frac{\partial}{\partial y}\left(\Gamma^\phi\frac{\partial\phi}{\partial y}\right) + S^\phi \tag{11}$$

where Γ^ϕ is an effective diffusion coefficient and S^ϕ denotes the source term. When new independent variables ξ and η are introduced, Eq. (11) changes according to the general transformation $\xi = \xi(x,y)$, $\eta = \eta(x,y)$. Partial derivatives of any function f are transformed according to

$$f_x = (y_\eta f_\xi - y_\xi f_\eta)/J \qquad f_y = (-x_\eta f_\xi + x_\xi f_\eta)/J \tag{12a}$$

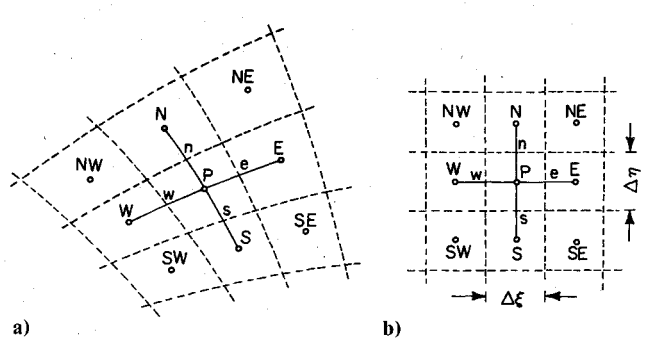

Fig. 1 Finite difference grid representation. a) Physical plane. b) Transformed plane.

where J is the Jacobian of the transformation given by

$$J=x_\xi y_\eta - x_\eta y_\xi \tag{12b}$$

Since the strong conservative form of the equation is desirable for numerical computations, the integral form of the conservational equations over a finite volume element is preferable. Upon introducing

$$G_1=uy_\eta - vx_\eta, \qquad G_2=vx_\xi - uy_\xi \tag{13}$$

$$\alpha=x_\eta^2+y_\eta^2, \qquad \beta=x_\xi x_\eta + y_\xi y_\eta, \qquad \gamma=x_\xi^2+y_\xi^2 \tag{14}$$

the following integral conservation relation is obtained from Eq. (11) for an arbitrary scalar dependent variable ϕ:

$$\int_B \{\rho G_1 \phi \mathrm{d}\eta - \rho G_2 \phi \mathrm{d}\xi\} = \int_B \{(\Gamma^\phi/J)(\alpha\phi_\xi - \beta\phi_\eta)\mathrm{d}\eta - (\Gamma^\phi/J)(\gamma\phi_\eta - \beta\phi_\xi)\mathrm{d}\xi\} + \int\int_R S^\phi J \mathrm{d}\xi \mathrm{d}\eta \tag{15}$$

Here G_1 and G_2 are directly related to the contravariant velocity components. In fact, $G_1/(\alpha)^{1/2}$ and $G_2/(\gamma)^{1/2}$ represent the velocity components normal to the lines of constant ξ and η, respectively, in the physical plane.

Method of Computation

General Transport Equations

In terms of the notation shown in Fig. 1 for a typical grid node P enclosed in its cell and surrounded by its neighbors N, S, E, and W, the finite difference approximation to the integral conservation relation, Eq. (15), over the cell is written as

$$(\rho G_1 \phi \Delta\eta)_w^e + (\rho G_2 \phi \Delta\xi)_s^n = \left\{\frac{\Gamma^\phi}{J}(\alpha\phi_\xi - \beta\phi_\eta)\Delta\eta\right\}_w^e + \left\{\frac{\Gamma^\phi}{J}(\gamma\phi_\eta - \beta\phi_\xi)\Delta\xi\right\}_s^n + S^\phi J \Delta\xi\Delta\eta \tag{16}$$

where ϕ is the unknown. In the present scheme, all flow properties are defined only at the nodes P, E, W, N, and S. Thus, in general the following approximations are made for the above finite difference expression, Eq. (16).

$$\rho G_1 \phi \Delta\eta|_c \approx (\rho G_1 \Delta\eta)_e \frac{1}{2}(\phi_P + \phi_E)$$
$$\frac{\Gamma^\phi}{J}(\alpha\phi_\xi)\Delta\eta|_e \approx \left(\frac{\Gamma^\phi}{J}\alpha\Delta\eta\right)_e (\phi_P - \phi_E)/\Delta\xi \tag{17}$$

Quantities such as $(\rho G_1 \Delta\eta)_e$ and $(\Gamma/J\alpha\Delta\eta)_e$ are obtained by linear interpolation in the physical plane. Substituting all relations of the type of Eq. (17) into Eq. (16), a relation between ϕ_P and the neighboring values is obtained, i.e.,

$$A_P\phi_P = A_E\phi_E + A_W\phi_W + A_N\phi_N + A_S\phi_S + S^\phi J\Delta\xi\Delta\eta - \left[\left(\frac{\Gamma^\phi}{J}\beta\phi_\eta\Delta\eta\right)_w^e + \left(\frac{\Gamma^\phi}{J}\beta\phi_\xi\Delta\xi\right)_s^n\right] \tag{18}$$

where the coefficients A involve the flow properties of convection, diffusion, area, etc. These coefficients are later modified according to a "hybrid scheme,"[7] which evaluates the convective term by the first-order upwind-differencing scheme whenever the grid cell Reynolds number (e.g., $\rho|G_1|J\delta\xi/\alpha\Gamma^\phi$) is greater than 2. The details can be found in Ref. 13. The terms within the bracket in Eq. (18) are originated from cross derivatives in the diffusion terms and are the results of the nonorthogonal coordinate system. These terms are usually very small and can be combined with the source term and treated as known quantities. They are evaluated from updated values through the following finite difference approximation

$$\frac{\Gamma^\phi}{J}\beta\phi_\eta\Delta\eta|_e = \left(\frac{\Gamma^\phi}{J}\beta\Delta\eta\right)_e \frac{1}{4}(\phi_{NE} - \phi_{SE} + \phi_N - \phi_S) \tag{19}$$

Pressure Correction Equation

An equation for the remaining unknown pressure is established by combining the continuity and momentum equations. For a simple scheme, the pressure correction can be derived from the momentum finite difference equations. To explain this procedure in some detail, it is assumed that a preliminary set of velocity components, u and v, are obtained from

$$u_P^* = \sum_{EWNS} A^u u^* + S_i^u + (B^u p_\xi^* + C^u p_\eta^*)$$
$$v_P^* = \sum_{EWNS} A^v v^* + S_i^v + (B^v P_\xi + C^v p_\eta^*) \tag{20}$$

where

$$B^u = \frac{-y_\eta \Delta\xi\Delta\eta}{A_P}, \qquad C^u = \frac{y_\xi \Delta\xi\Delta\eta}{A_P}$$
$$B^v = \frac{x_\eta \Delta\xi\Delta\eta}{A_P}, \qquad C^v = \frac{-x_\xi \Delta\xi\Delta\eta}{A_P}$$

and S_i^u and S_i^v are residues from S^u, S^v after the pressure gradient terms have been extracted from them. The superscript * for u and v denotes that they are based on the estimated pressure field p^*. In general, u^* and v^* will not satisfy the continuity equation. Instead a net mass source is produced. To remove this mass source, the velocity components are assumed to be corrected by the relations

$$u = u^* + (B^u p_\xi' + C^u p_\eta') \tag{21a}$$

$$v = v^* + (B^v p_\xi' + C^v p_\eta') \tag{21b}$$

where p' is the pressure correction which is related to the pressure p according to

$$p = p^* + p' \tag{21c}$$

Subsequently, the correction equations for G_1 and G_2 are obtained from Eq. (13), i.e.,

$$G_1 = G_1^* + (B^u y_\eta - B^v x_\eta)p_\xi' + (C^u y_\eta - C^v x_\eta)p_\eta' \tag{22a}$$

$$G_2 = G_2^* + (C^v x_\xi - C^u y_\xi)p_\eta' + (B^v x_\xi - B^u y_\xi)p_\xi' \tag{22b}$$

where again G_1^* and G_2^* are based on u^* and v^*.

It is noted that the last two terms of Eqs. (22a) and (22b) are negligible if the grid system is nearly orthogonal. One may, therefore, further simplify the above expressions by neglecting these terms, and the result becomes

$$G_1 = G_1^* + Bp_\xi' \qquad G_2 = G_2^* + Cp_\eta' \tag{23}$$

where $B = B^u y_\eta - B^v x_\eta$ and $C = C^v x_\xi - C^u y_\xi$.

One may expect that this highly approximate relation, Eq. (23), leads to the establishment of the correct pressure field

after consideration of the following. If the solution converges, the correction terms at the final converged state should vanish, and the converged solution, nevertheless, satisfies the basic Eq. (20). The correction equations thus do not have to be rigorously derived from Eq. (20). This form is preferred because of its simplicity and better convergence properties. Upon substituting Eq. (23) into the continuity equation, one obtains a Poisson equation for the pressure correction, i.e.,

$$(\rho Bp'_\xi \Delta\eta)_e - (\rho Bp'_\xi \Delta\eta)_w + (\rho Cp'_\eta \Delta\xi)_n - (\rho Cp'_\eta \Delta\xi)_s + m_p = 0 \tag{24}$$

where m_p is the integrated mass source from u^* and v^* established for the element under consideration.

With the second-order center-difference approximations for the pressure gradients on the cell boundaries, the finite difference form of Eq. (24) is

$$A^p_P p'_P = A^p_E\, p'_E + A^p_W p'_W + A^p_N p'_N + A^p_S p'_S + S \tag{25}$$

where coefficients A involve coefficients B, C, density, etc., and S represents the local imbalance of mass. Equation (25) can now be solved with the same algorithm for Eq. (18) to yield the corrective pressure. Thus, the pressure and velocity components are corrected according to Eq. (21).

It has been learned from this pressure correction scheme with the ordinary grid arrangement, that the oscillatory pressure field is produced. This has been observed previously by others.[14] The major source of this instability originated from the second-order centered $2\Delta X$-difference approximation of the pressure gradient at the grid node. This scheme cannot sense the $1\Delta X$-pressure oscillation. A staggered mesh was successfully used by many[7-9] to remove these oscillations since the centered $1\Delta X$-difference could be used for the pressure gradient with the staggered arrangement. However, this technique cannot be applied to the present method since the Cartesian velocity components u and v are not related to the grid line orientations. As an alternative approach, the scheme of Hirt et al.,[10] where the pressure is defined in the center of the cell, while u and v velocity components are defined at all corners, was introduced. In this case, pressure oscillation remained in the diagonal direction, and this scheme is equally unsuitable for the present purpose.

To eliminate the oscillations with the present ordinary grid arrangement, a new treatment of the locally linearized convective terms, G_1 and G_2, was introduced. It should be remembered that these convective terms are always located on the cell boundaries and are obtained by interpolations between grid nodes. These interpolations were responsible for decoupling the velocity and pressure fields. If G_1^* were derived from Eq. (13), where u^* and v^* were obtained from Eq. (20), it would assume the expression

$$G_1^* = Bp_\xi^* + \ldots \tag{26}$$

where all other terms are dropped for the convenience of discussion. Even though G_1^* is related to p_ξ^* in the form of Eq. (26), the G_1^* value on the cell boundary is actually obtained from interpolation between the grid nodes. Thus the G_1 value so determined cannot detect $1\delta\xi$-pressure variation. One may remedy this situation by correcting the p_ξ^* term through a $1\delta\xi$-difference scheme on the cell boundary. The effective form was found to be

$$G_{1_e}^* = \overline{G_1^*} + \overline{B}\left(\frac{p_E^* - p_P^*}{\delta\xi} - \overline{p_\xi^*}\right) \tag{27}$$

where the overbar denotes the regular results obtained from linear interpolation between grid nodes E and P. The interpolated pressure gradient term p_ξ^* based on the $2\delta\xi$-center difference is replaced by the $1\delta\xi$-center difference on the cell boundary. This procedure ensures strong velocity-pressure coupling. In some test cases, this procedure was proven to show better convergence behavior than the original SIMPLE procedure. It is worthwhile to note that this modification through Eq. (27) becomes redundant if the pressure varies linearly within the field.

The boundary condition required to solve the pressure correction equation is that the normal derivative of the pressure correction p' vanishes on the boundary in the computational plane. The actual pressure value on the boundary is established by extrapolation from interior values with the conditions of vanishing normal derivatives of pressure there.

Solution Procedure

The overall solution procedure is similar to that of the SIMPLE procedure.[7] A field of intermediate velocity components, u^* and v^*, is obtained by solving the momentum equations, Eqs. (20), using a preliminary pressure field. Subsequently, the continuity constraint is enforced from setting up an equation of the corrective pressure p'. By solving the resulting equation, Eq. (25), the required adjustments to the pressure and velocity components are determined. Equation (18) for the remaining scalar variables, k and ϵ, are solved in turn. This process is defined as one iteration cycle and is repeated until a converged solution is obtained. Convergence is reached for vanishing mass sources (within an arbitrarily small margin) throughout the computational domain.

Generation of the Coordinate System

The grid generation scheme developed by Sorenson and Steger[15] is adopted in the present study. In this method, the curvilinear coordinates are generated by solving the elliptic equations

$$\alpha x_{\xi\xi} - 2\beta x_{\xi\eta} + \gamma x_{\eta\eta} = 0 \qquad \alpha y_{\xi\xi} - 2\beta y_{\xi\eta} + \gamma y_{\eta\eta} = 0 \tag{28}$$

After the grid is constructed, a simple exponential stretching technique is used to cluster points near the airfoil surface. This is done in order to resolve the high gradient flow within the boundary layer. In the present study, an additional modification is made to eliminate the coordinate slope discontinuity in the wake region, shown in Fig. 2a. The discontinuity is removed by fitting fourth-order polynomials across the cut. The resulting grid system is illustrated in Fig. 2b. With this modification, the grid points along the cut can be treated as regular interior nodes.

Results and Discussion

The objective of the present work is the study of turbulent flow over an isolated airfoil and correlation of the computed results with experimental data. Before any effort of this

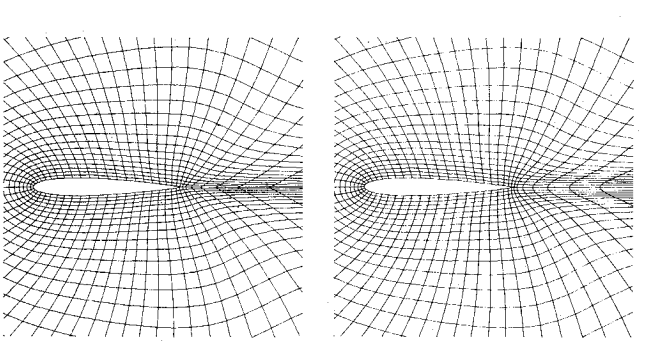

a) b)

Fig. 2 Grid detail near body. a) After reclustering. b) After partial reconstruction.

nature was carried out, a variety of laminar flow cases, ranging from a flow past a circular cylinder to a flow past an NACA 0012 airfoil at low Reynolds number, was computed to check the numerical accuracy of the computer program so developed. The results were all satisfactory when compared with those previously published.

The experimental data of turbulent flow past isolated airfoils are not abundantly available at the present time. Recently, Hah and Lakshminarayana[6] carried out experimental investigations of an NACA 0012 airfoil at several angles of incidence. Coles and Wadcock[16] tested an NACA 4412 airfoil at a maximum lift condition with a 13.87 deg angle of attack. The present effort was aimed at the computation of these flow conditions for which experimental data were available for comparison. However, it is noted that there is no single set of experimental data covering the entire flowfield. The experimental data by Hah and Lakshminarayana[6] were restricted to the near-wake region. The experimental data by Coles and Wadcock[16] covered only the rear part of the suction surface and the near-wake region, although the pressure distribution around the whole airfoil surface was reported. The surface pressure data by Gregory and O'Reilly[17] for an NACA 0012 airfoil were also available for comparison.

Results for an NACA 0012 Airfoil without Separation at $Re_C = 2.8 \times 10^6$

As a preliminary effort, the external flow past an NACA 0012 airfoil was considered at $Re_C = 2.8 \times 10^6$. A 77×34 grid was used and 49 grid points were distributed over the airfoil. The front and rear outer boundaries were located eight chord lengths away from the body, and the top and bottom outer boundaries were located at 12 chord lengths from the body. The velocity was set to freestream value over the front, top, and bottom outer boundaries. On the rear outer boundary, which was normal to the airfoil chord line, the velocity components and the turbulent scalars were extrapolated from the inner solution by assuming that the first derivatives of flow properties along the $\eta = \text{const}$ lines vanish. The velocity profile normal to the exit plane was then adjusted to satisfy the principle of global conservation of mass.

0 deg Angle of Attack

The computation was performed in the whole domain even for 0 deg incidence to avoid numerical errors from extrapolation along the line of symmetry. The surface pressure distribution is plotted in Fig. 3 and compared with the experimental data by Gregory and O'Reilly,[17] and the computational results by Shamroth and Gibeling.[4] In general, the pressure distribution shows good agreement with the experimental data. Slight discrepancies are shown near the leading and trailing edges. The minimum pressure near the leading edge was underestimated and a lower pressure was predicted in the trailing edge region. Two possible reasons for these discrepancies are given. First, the boundary-layer growth was not accurately predicted because of inadequate turbulence modeling. Second, the grid spacing in the leading and trailing edge regions was not sufficiently fine to resolve the strong gradients in those regions.

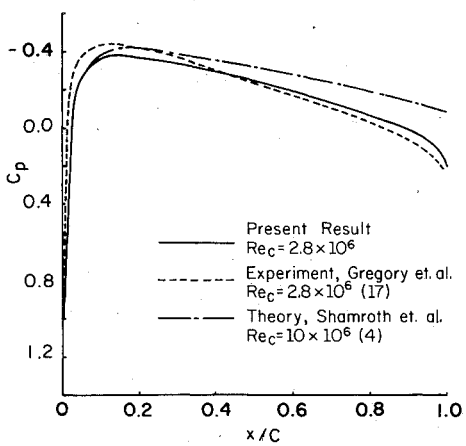

Fig. 3 Surface pressure distribution for NACA 0012 airfoil at zero incidence ($Re_C = 2.8 \times 10^6$).

6 deg Angle of Attack

In this case, all the parameters in the computation were kept the same as the previous case except the airfoil is rotated through 6 deg. The calculated surface pressure distribution is plotted in Fig. 4 along with the experimental data from Ref. 17 and the computational results from Ref. 4. Again, the agreement with the data is good except in the leading and trailing edge regions. It is anticipated that a finer grid in those regions would substantially improve the accuracy of the present results.

Flow Past an NACA 0012 Airfoil without Separation at $Re_C = 3.8 \times 10^5$

The flow over the NACA 0012 airfoil at 6 deg incidence was calculated for $Re_C = 3.8 \times 10^5$ and the results were compared with the experimental data of Hah and Lakshminarayana. The wind tunnel blockage effect was accounted for by treating the computational outer boundaries as the physical locations of the wind tunnel wall which was located at three chord lengths away from the body. The front and rear outer boundaries were located three and five chord lengths away from the body. The front inlet boundary was defined by half of the circular arc. An 87×30 grid was used with 59 points distributed over the airfoil surface. The grid spacing in the η direction along the airfoil was 0.0025 chords. The treatment of the boundary conditions was essentially the same as that in the previous computations. The boundary-layer development

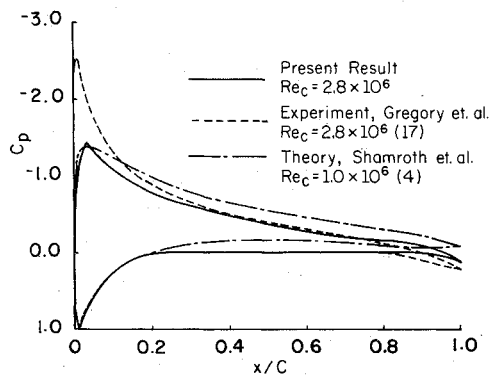

Fig. 4 Surface pressure distribution for NACA 0012 airfoil at 6 deg incidence ($Re_C = 2.8 \times 10^6$).

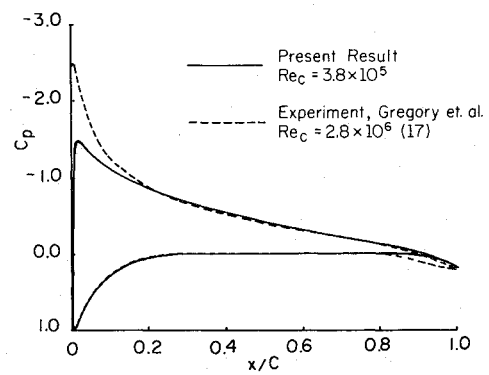

Fig. 5 Surface pressure distribution for NACA 0012 airfoil at 6 deg incidence ($Re_C = 3.8 \times 10^5$).

on the wind tunnel wall was neglected and a simple slip boundary condition was applied.

Figure 5 shows the calculated surface pressure distribution. Some improvement in the accuracy of the results over those presented in Fig. 4 can be observed at the leading and trailing edges. This is probably the result of the finer grid used in this case. Some discrepancies still remain where excessively high gradients exist. It is speculated that the discrepancy near the leading edge results from inadequate resolution since inviscid flow governs the flow process there. While inadequate resolution is considered to be the dominant source of error near the leading edge, the effect of inadequate turbulence modeling becomes equally important near the trailing edge region. There, the boundary layers on both the upper and lower surfaces have considerable thickness and, therefore, significantly modify the pressure distribution. The shear-layer interaction and the subsequent relaxation process dominate the flow events downstream of the trailing edge which can also alter the upstream flow conditions. Another problem with the present approach was found in the near-wake region. Although it is well known that the mean flow behavior within the wake is entirely different from the wall turbulent flows, the effect of the upstream logarithmic profile should have persisted within the immediate near wake and the present approach cannot account for this effect. The grid spacing extending from the airfoil boundary layers was not fine enough to allow an adequate description of such a near-wake profile, thus some error in evaluating the shear stress along the wake centerline occurred.

Streamlines for this example problem are plotted in Fig. 6. The streamlines indicate a thicker viscous layer on the suction surface. The u-velocity component and Reynolds shear stress profiles are plotted at different x locations in Fig. 7. These results indicate turbulent structural behavior in the boundary layer and the near-wake regions. Downstream of the trailing edge, the near-wake profile undergoes a fast relaxation process. In this region, relatively high Reynolds stresses are produced due to high mean shear and eventually they are reduced due to the diffusive and dissipative nature of the process. A detailed comparison with the experimental data[6] for the near wake was not attempted since the present approach involves some errors in the near-wake flow as previously discussed. However, the evaluation of the wake centerline velocity is presented and compared with the experimental data in Fig. 8. Reasonably good correlation is shown between the data sets.

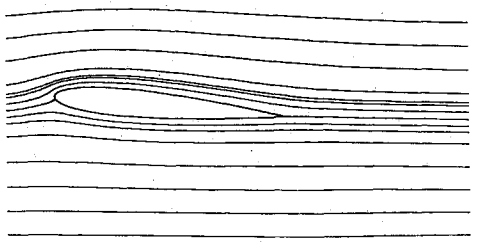

Fig. 6 Streamlines for NACA airfoil at 6 deg incidence ($Re_C = 3.8 \times 10^5$).

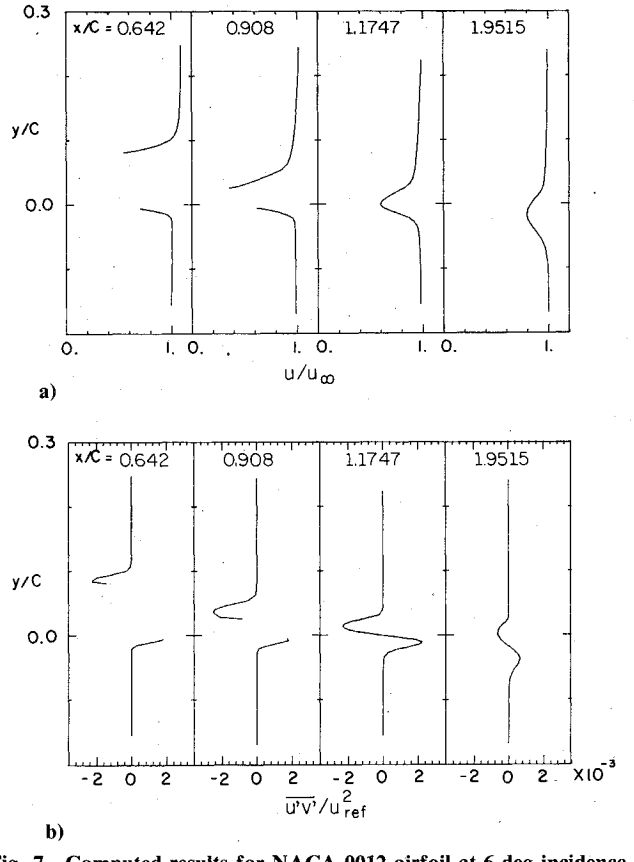

Fig. 7 Computed results for NACA 0012 airfoil at 6 deg incidence ($Re_C = 3.8 \times 10^5$). a) u-velocity profiles. b) $\overline{u'v'}$ profiles.

Flow Past an NACA Airfoil with Separation at $Re_C = 1.5 \times 10^6$

A major part of this study was aimed at the prediction of the flow past an NACA 4412 airfoil at a maximum lift condition with a 13.87 deg angle of attack. The blockage effect of the confined wind tunnel test section was simulated in the computations. The computational domain was defined as illustrated in Fig. 9. All the lengths were nondimensionalized by the airfoil chord. The converging and diverging tunnel wall section were defined with $\alpha = \beta = 4$ deg.

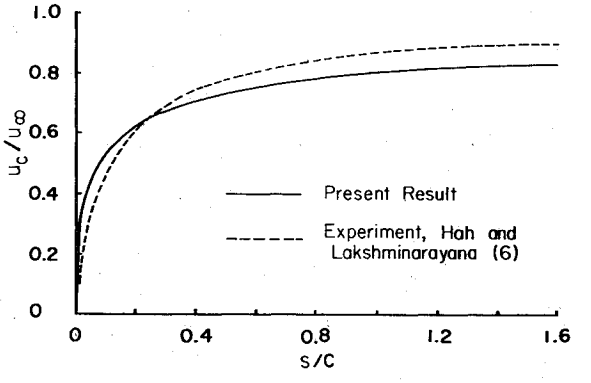

Fig. 8 Evolution of the wake center velocity for NACA 0012 airfoil at 6 deg incidence ($Re_C = 3.8 \times 10^5$).

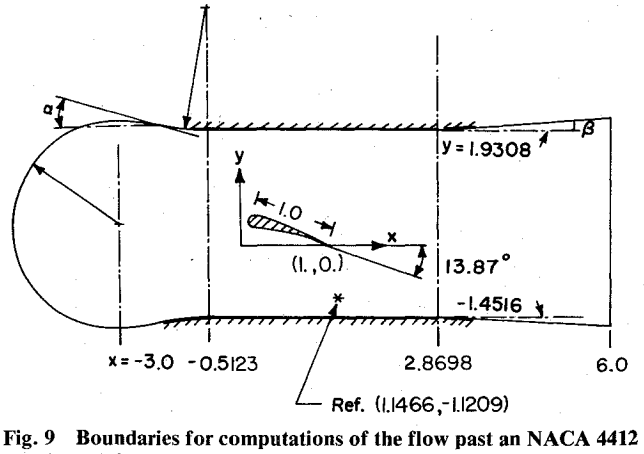

Fig. 9 Boundaries for computations of the flow past an NACA 4412 airfoil at 13.87 deg incidence.

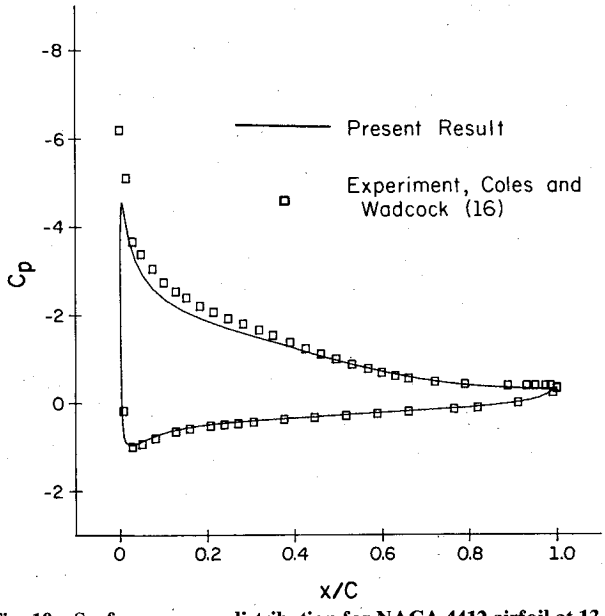

Fig. 10 Surface pressure distribution for NACA 4412 airfoil at 13.87 deg incidence ($Re_C = 1.5 \times 10^6$).

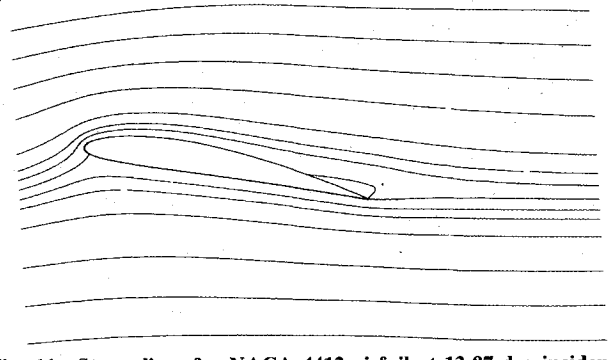

Fig. 11 Streamlines for NACA 4412 airfoil at 13.87 deg incidence ($Re_C = 1.5 \times 10^6$).

The computation was performed on a 95×31 grid with 63 points distribution along the airfoil surface. Uniform approaching freestream conditions were imposed on the front outer boundary. Wake profile boundary condition simulation at the exit plane of the diverging diffuser section was abandoned due to numerical difficulties. Instead, a uniform velocity profile was imposed. Virtually no influence of this rear outer boundary condition was observed on the inner solution near the airfoil. The slip boundary conditions were imposed on the wind tunnel walls.

The calculated surface pressure distribution, plotted in Fig. 10, shows very good agreement with the experimental data. The discrepancies shown near the leading edge are attributed to inadequate resolution of the strong gradient in that region. In the preliminary computations, the successive grid refinements gave consistently improved results. Unfortunately, further grid refinement was not possible because of the limitation on computer storage. Figure 11 shows the streamlines and velocity vectors from the computation. These results clearly show the trailing edge separation bubble. The free streamlines were modified due to the displacement effect of the bubble, which, in turn, altered the airfoil surface pressure distribution. Detailed velocity component profile and Reynolds shear stress profiles are given in Fig. 12 along with the experimental data. The results are plotted vs distance normal to the airfoil chordline. The discrepancies between the predicted and experimentally determined mean velocity

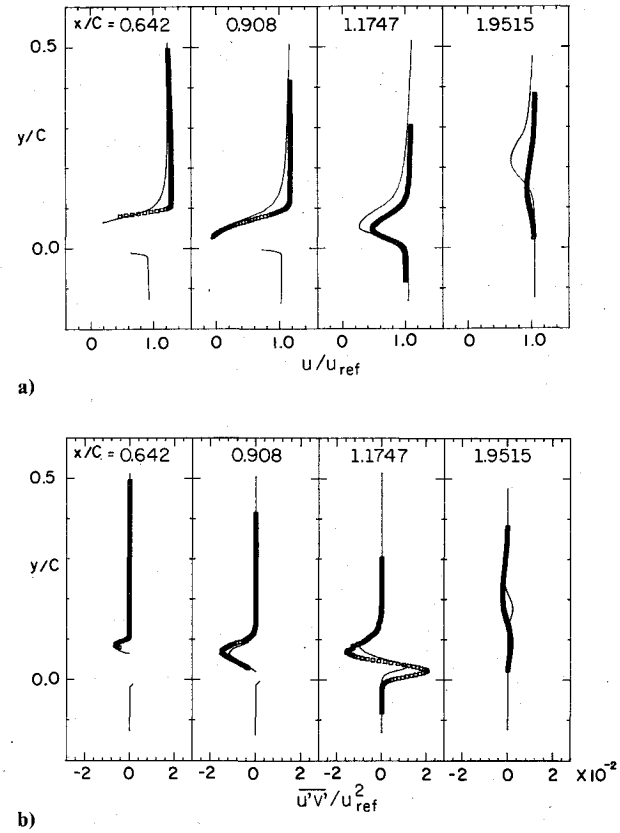

Fig. 12 Results for NACA 4412 airfoil at 13.87 deg incidence ($Re_C = 1.5 \times 10^6$): ——, presented result; □, experiment (Ref. 16).

profiles in Fig. 12a are attributed to inadequate grid refinement and possibly inadequate turbulence modeling.

The predicted downstream near-wake profile after the trailing edge generally shows lower minimum wake velocities and larger wake widths than indicated in the experimental results. This suggests that the mixing is less active in the near wake, and that the rapid development of the wake is suppressed. This trend was also observed by Pope and Whitelaw[5] in the computation of separated flows using the k-ϵ model.

It is premature to make any firm assessment on the k-ϵ turbulence model with the present study since the grid refinement was not sufficient to obtain the grid independent results. However, some remarks can be made on the turbulence model. The k-ϵ model is based on simple flows such as channel Couette flow and the decaying isotropic grid turbulence. The capability of the k-ϵ model is naturally in doubt for the complex separated flows. The qualitative picture of the present prediction is in accordance with what has been reported in Ref. 5. Once again it is confirmed that a better turbulence model is required for the accurate quantitative predictions. The suitability of the wall function method for the present application needs to be investigated further.

All of the computations were initialized with the freestream flow conditions. Generally, good convergence behavior was observed. The calculations were made on a CYBER 175 computer. The time and storage requirements of the Fortran computer program were 0.00083 s/grid node/iteration and 23,440 words plus 37.8 words/grid node, respectively. About 500 iterations were needed for the case without separation and twice as many iterations were required for the case with separation.

Conclusion

A finite volume method for the calculation of recirculating turbulent flows in general curvilinear coordinates was developed. Attached and separated flows over an isolated

airfoil were calculated using the standard k-ϵ turbulence model. Detailed comparisons on the predicted result and experimental data were made for the wakes and separated flow regions. It was determined that the accuracy of the results was highly dependent on degree of resolution of the strong leading and trailing edge gradients. Without separation, the k-ϵ turbulence model predicted values in reasonably good agreement with the experimental data. With separation, the k-ϵ turbulence model predicted poor results even though fairly good pressure distribution on the airfoil and reasonable overall behavior were predicted. The requirement of the better turbulence model is indicated.

Acknowledgments

This work was conducted at the University of Illinois at Urbana-Champaign with partial support from U.S. Army Research Office through Grant DAAG 29-79-C-184. The authors would also like to express their thanks to Dr. D. Sharma for sharing his knowledge on the SIMPLE method.

References

[1] Wu, J. C., Sampath, S., and Sankar, N. L., "Dynamic Stall of an Oscillating Airfoil," *Proceedings of AGARD Conference on Unsteady Aerodynamics*, NATO, Advisory Group of Aero. Research & Development, 1977, pp. 24-1 to 24-18.

[2] Steger, J. L., "Implicit Finite Difference Simulation of Flow About Arbitrary Two-Dimensional Geometries," *AIAA Journal*, Vol. 16, July 1978, pp. 679-686.

[3] Gibeling, H. J., Shamroth, S. J., and Eiseman, P. R., "Analysis of Strong Interaction Dynamic Stall for Laminar Flow of Airfoils," NASA CR-2969, 1978.

[4] Shamroth, S. J. and Gibeling, H. J., "The Prediction of the Turbulent Flow Field about an Isolated Airfoil," AIAA Paper 79-1543, 1979.

[5] Pope, S. B. and Whitelaw, J. H., "The Calculation of Near-Wake Flow," *Journal of Fluid Mechanics*, Vol. 73, Pt. 1, Jan. 1976, pp. 9-32.

[6] Han, C. and Lakshminarayana, B., "Prediction of Two- and Three-Dimensional Asymmetrical Turbulent Wakes, Including Curvature and Rotation Effects," *AIAA Journal*, Vol. 18, Oct. 1980, pp. 1196-1204.

[7] Caretto, L. S., Gosman, A. D., Patankar, S. V., and Spalding, D. B., "Two Calculation Procedures for Steady, Three-Dimensional Flows with Recirculation," *Proceedings of the Third International Conference on Numerical Methods in Fluid Dynamics*, Springer-Verlag, 1972, pp. 60-68.

[8] Pope, S. B., "The Calculation of Turbulent Recirculating Flows in General Orthogonal Coordinates," *Journal of Computational Physics*, Vol. 26, No. 2, 1978, pp. 197-217.

[9] Demirdzic, I., Gosman, A. D., and Issa, R. I., "A Finite-Volume Method for the Prediction of Turbulent Flow in Arbitrary Geometries," Paper presented at 7th International Conference on Numerical Methods in Fluid Dynamics, Stanford University and NASA Ames, June 1980.

[10] Hirt, C. W., Amsden, A. A., and Cook, J. L., "An Arbitrary Lagrangian-Eulerian Computing Method for All Flow Speeds," *Journal of Computational Physics*, Vol. 14, No. 3, 1974, pp. 227-253.

[11] Jones, W. P. and Launder, B. E., "The Prediction of Laminarization with a Two-Equation Model of Turbulence," *International Journal of Heat and Mass Transfer*, Vol. 15, Feb. 1972, pp. 301-314.

[12] Launder, B. E. and Spalding, D. B., "The Numerical Calculation of Turbulent Flows," *Computer Methods in Applied Mechanics and Engineering*, Vol. 3, No. 2, 1974, pp. 269-289.

[13] Rhie, C. M., "A Numerical Study of the Flow Past an Isolated Airfoil with Separation," Ph.D. Thesis, Dept. of Mechanical and Industrial Engineering, University of Illinois at Urbana-Champaign, 1981.

[14] Rubin, S. J. et al., "Numerical Studies of Incompressible Viscous Flow in a Driven Cavity," NASA SP-378, 1975.

[15] Sorenson, R. L. and Steger, J. L., "Simplified Clustering of Nonorthogonal Grids Generated by Elliptic Partial Differential Equations," NASA TM 73252, 1977.

[16] Coles, D. and Wadcock, A. J., "Flying Hotwire Study of Flow Past an NACA 4412 Airfoil at Maximum Lift," *AIAA Journal*, Vol. 17, April 1979, pp. 321-329.

[17] Gregory, N. and O'Reilly, C. L., "Low Speed Aerodynamic Characteristics of NACA 0012 Airfoil Section, Including the Effects of Upper Surface Roughness Simulation Hoarfrost," National Physical Laboratory, Teddington, England, Aero Rept. 1308, 1970.